PHILOSOPHICAL TRANSACTIONS OF THE ROYAL SOCIETY A MATHEMATICAL, PHYSICAL & ENGINEERING SCIENCES

Magic Angle Spinning in Solid State n.m.r. Spectroscopy

E. R. Andrew

Phil. Trans. R. Soc. Lond. A 1981 **299**, 505-520
doi: 10.1098/rsta.1981.0032

Phil. Trans. R. Soc. Lond. A **299**, 505–520 (1981)
Printed in Great Britain

Magic angle spinning in solid state n.m.r. spectroscopy

By E. R. Andrew
Department of Physics, University of Nottingham, University Park, Nottingham NG7 2RD, U.K.

Rapid specimen rotation about an axis inclined at the 'magic angle' of 54° 44′ to the Zeeman field direction can remove many sources of broadening from the n.m.r. spectrum of a solid and enable finer features to be revealed. In this paper the basic principles of magic angle spinning are given and the effects on the chemical shift interaction, the magnetic dipolar and pseudo-dipolar interactions, both homonuclear and heteronuclear, and the electric quadrupolar interactions are examined. The anisotropic parts of these interactions are removed from the central spectrum and appear as spinning sidebands. The interactions that remain are the isotropic shifts and J couplings as in isotropic fluids. Examples of the effects of magic angle spinning on a variety of interactions are given. When applied to metals the anisotropy of Knight shift is removed, isotropic Knight shifts may be measured with precision, and the Ruderman–Kittel interaction may be determined in the presence of a much larger dipolar interaction. The effects of spinning on homogeneous and inhomogeneous spectra are distinguished. Sources of residual broadening are identified.

Magic angle spinning may be used on its own, and may also be successfully combined with multiple-pulse and double resonance n.m.r. methods to obtain high-resolution n.m.r. spectra of powders and polymers.

1. Introduction

One of the most striking and characteristic features of nuclear magnetic resonance (n.m.r.) is that the spectra from solids are so very much broader than those from liquids. An excellent example is provided by water whose proton n.m.r. linewidth at room temperature is about 0.1 Hz, while for ice at low temperatures it is about 10^5 Hz, six orders of magnitude broader. The well understood origin of this substantial difference in behaviour lies in the static anisotropic interactions to which the nuclei in the solid are subject. In mobile fluids the rapid isotropic motions of the nuclei average the anisotropic interactions and effectively remove them from the spectrum. As a consequence, a rich high-resolution n.m.r. spectrum is often revealed that is of great value in the structural and dynamical analysis of molecules.

In solids, too, there is often sufficient motion of the nuclei to narrow the n.m.r. spectra substantially, and sometimes the spectrum is sufficiently narrowed to resolve a high-resolution n.m.r. spectrum. An example is the ^{31}P n.m.r. spectrum of polycrystalline P_4S_3 at 420 K, 26 K below its melting point, shown in figure 1 (Andrew *et al.* 1974*c*, 1978). An AB_3 spectrum is resolved, the doublet arising from the three basal phosphorus nuclei in the molecule and the quartet coming from the apical nucleus. The J coupling constant and the chemical shift separation were determined.

However, in more general cases sufficient motion is not present in solids to narrow the n.m.r. lines, and in this situation one may seek to emulate Nature by imposing a motion on the nuclei. This was first done by rapidly spinning the solid specimen (Andrew *et al.* 1958*a*, *b*, 1959; Andrew 1959; Lowe 1959). A few years later an alternative approach was developed by imposing a motion on the nuclei in spin space (Mansfield & Ware 1966; Ostroff & Waugh 1966),

as discussed in the two previous papers in this symposium (by Mansfield and Haeberlen). At one time these two techniques were seen as competitive approaches to line-narrowing in solids, but now they are seen very much as complementary methods. In particular, for polycrystalline and amorphous materials, which cover most of the materials of practical interest, sharp highly resolved spectra, comparable with those from fluids, can only be obtained with the use of magic angle spinning, which removes anisotropic sources of broadening which resist averaging in spin space, as discussed in the paper by Gerstein (this symposium). In the same way, double resonance methods for rare spins such as ^{13}C, ^{15}N and ^{29}Si (Pines *et al.* 1972; Pines, this symposium) also require the addition of magic angle spinning to obtain the highest resolution (Schaefer & Stejskal 1976; Lippmaa *et al.* 1976, Schaefer *et al.*, this symposium; Garroway *et al.*, this symposium; Balimann *et al.*, this symposium). For these reasons, modern commercial n.m.r. spectrometers for work with solids normally include a magic angle spinning facility.

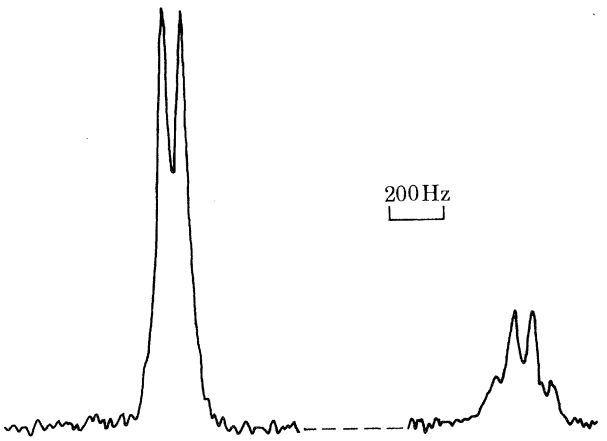

FIGURE 1. ^{31}P n.m.r. spectrum in polycrystalline P_4S_3 at 420 K (melting point 446 K). The spectrum is strongly narrowed by molecular motion in the solid and displays an AB_3 type fine structure (Andrew *et al.* 1974*c*).

In this paper the essential features of magic angle spinning are set out. Examples are given of its effectiveness in n.m.r. line narrowing when used alone, and this will serve as an introduction to later papers at this symposium in which the method is used in conjunction with other techniques. Earlier reviews of magic angle spinning and its effects in solid state n.m.r. have been given by Andrew (1970, 1971, 1975); the subject is also discussed in the books on high-resolution n.m.r. in solids by Haeberlen (1976) and Mehring (1976).

The anisotropic nuclear interactions that are of interest in solid state n.m.r. spectra are the following:

(1) direct magnetic dipolar: (*a*) homonuclear;
(*b*) heteronuclear;
(2) indirect electron-coupled: (*a*) homonuclear;
(*b*) heteronuclear;
(3) electric quadrupolar (for nuclei with spin $I > \frac{1}{2}$);
(4) electron shielding (chemical shift, Knight shift).

Consideration will now be given to the effect of magic angle spinning on each of these interactions.

2. Magic angle spinning and dipolar interactions

We begin by examining the effect of rapid specimen rotation on nuclear magnetic dipolar interactions since they are always present in some degree and were historically the first to be considered and removed; moreover this gives good insight to the operation of the method.

The truncated dipolar interaction Hamiltonian, for all nuclear pairs i, j in the solid, both like and unlike, is

$$\mathscr{H}_{\mathrm{d}} = \sum_{i<j} \tfrac{1}{2}\gamma_i\gamma_j\hbar^2 r_{ij}^{-3}(\boldsymbol{I}_i\cdot\boldsymbol{I}_j - 3I_{iz}I_{jz})\,(3\cos^2\theta_{ij}-1), \tag{1}$$

where γ_i, γ_j are the nuclear gyromagnetic ratios, $\boldsymbol{r}_{ij}$ is the internuclear displacement, and θ_{ij} is the angle between $\boldsymbol{r}_{ij}$ and the Zeeman field $\boldsymbol{H}_0$, which is directed along the z axis in the laboratory frame. The n.m.r. spectrum is in principle calculated by treating $\mathscr{H}_{\mathrm{d}}$ as a perturbation on the Zeeman term $\mathscr{H}_{\mathrm{Z}}$, where

$$\mathscr{H}_{\mathrm{Z}} = -\sum_i \gamma_i\hbar\boldsymbol{I}_i\cdot\boldsymbol{H}_0. \tag{2}$$

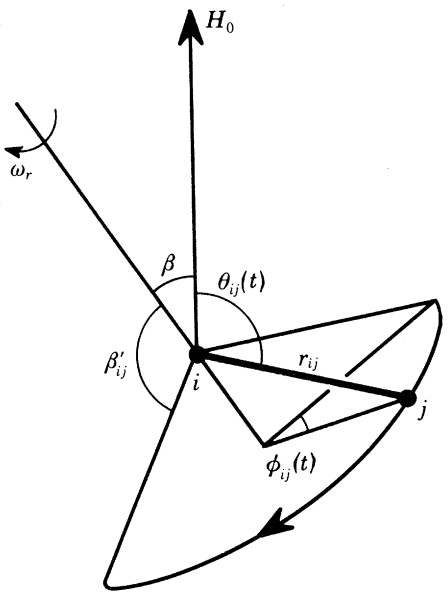

Figure 2. Diagram illustrating the motion of a typical internuclear vector $\boldsymbol{r}_{ij}$ when a solid is rotated with angular velocity ω_{r} about an axis inclined at angle β to $\boldsymbol{H}_0$.

Since the isotropic average $\overline{\cos^2\theta_{ij}} = \frac{1}{3}$, it follows from (1) that the isotropic average of the dipolar Hamiltonian, $\overline{\mathscr{H}_{\mathrm{d}}} = 0$, and rapid isotropic motion in fluids therefore eliminates the dipolar interaction from the n.m.r. spectrum.

If a solid specimen, whether monocrystalline, polycrystalline or amorphous, is rotated uniformly with angular velocity ω_{r} about an axis inclined to $\boldsymbol{H}_0$ at angle β, every internuclear vector $\boldsymbol{r}_{ij}$ in the solid describes a motion illustrated in figure 2. The angle θ_{ij} becomes time-dependent, and the factor $(3\cos^2\theta_{ij}-1)$ in (1) runs through a range of values that may be both positive and negative. Its average value may be made zero by judicious choice of β.

Expressing $\cos\theta_{ij}$ in terms of the other angles of the system,

$$\cos\theta_{ij} = \cos\beta\cos\beta'_{ij} + \sin\beta\sin\beta'_{ij}\cos(\omega_{\mathrm{r}}t + \phi_{0ij}), \tag{3}$$

we find after rearrangement that

$$\mathscr{H}_{\mathrm{d}}(t) = \sum_{i<j} \tfrac{1}{2}\gamma_i\gamma_j\hbar^2 r_{ij}^{-3}(\boldsymbol{I}_i\cdot\boldsymbol{I}_j - 3I_{iz}I_{jz})\,\{\tfrac{1}{2}(3\cos^2\beta - 1)\,(3\cos^2\beta'_{ij} - 1) + \tfrac{3}{2}\sin 2\beta\,\sin 2\beta'_{ij}\cos(\omega_{\mathrm{r}}t + \phi_{0ij}) + \tfrac{3}{2}\sin^2\beta\,\sin^2\beta'_{ij}\cos 2(\omega_{\mathrm{r}}t + \phi_{0ij})\}. \tag{4}$$

Notice that the first term in the curly bracket is constant, while the second and third terms are periodic with zero mean value. It is convenient to divide $\mathscr{H}_{\mathrm{d}}(t)$ into two terms, its mean value $\overline{\mathscr{H}}_{\mathrm{d}}$ and the remainder, which is periodic with zero mean value:

$$\mathscr{H}_{\mathrm{d}}(t) = \overline{\mathscr{H}}_{\mathrm{d}} + (\mathscr{H}_{\mathrm{d}} - \overline{\mathscr{H}}_{\mathrm{d}}). \tag{5}$$

The first term on the right-hand side is constant and gives a reduced dipolar interaction and the narrowed spectrum, while the second term, which is periodic in ω_{r} and $2\omega_{\mathrm{r}}$, gives rise to rotational sidebands at multiples of ω_{r}. We note that in the special case of $\beta = \frac{1}{2}\pi$ that since $\sin 2\beta = 0$, only even-order sidebands contribute. We see therefore that

$$\overline{\mathscr{H}}_{\mathrm{d}} = \tfrac{1}{2}(3\cos^2\beta - 1)\sum_{i<j}\tfrac{1}{2}\gamma_i\gamma_j\hbar^2 r_{ij}^{-3}(\boldsymbol{I}_i\cdot\boldsymbol{I}_j - 3I_{iz}I_{jz})\,(3\cos^2\beta'_{ij} - 1). \tag{6}$$

If we now compare (1) and (6) we see that for polycrystalline and amorphous material the spectrum retains an identical shape, but is reduced in width by the scale factor

$$F(\beta) = |\tfrac{1}{2}(3\cos^2\beta - 1)|. \tag{7}$$

The second moment of the narrowed spectrum is reduced by $F^2(\beta)$. On the other hand, one can show that the second moment of the whole spectrum, including sidebands, is unchanged, expressing the expected invariance of the second moment of the whole spectrum (Andrew *et al.* 1958*a*, *b*; Andrew & Newing 1958; Andrew & Jenks 1962).

Let us note some particular values of $F(\beta)$:

For $\beta = 0$, $F(\beta) = 1$;

$\beta = \frac{1}{2}\pi$, $F(\beta) = \frac{1}{2}$;

$\beta = \arccos\frac{1}{\sqrt{3}} = 54^\circ\,44'\,8''$, $F(\beta) = 0$.

Rotation about $\boldsymbol{H}_0$ has no effect, rotation about an axis normal to $\boldsymbol{H}_0$ halves the spectral width, while rotation about an axis making the magic angle† of 54° 44′ should reduce the dipolar broadening to zero.

These predictions were found to be borne out experimentally. The first experiments were made with ^{23}Na n.m.r. in sodium chloride. A single crystal was used to prevent any significant quadrupolar broadening due to strains or other defects in this cubic crystal. The second moment from the static crystal agreed within experimental error with the value of $0.55\,G^2$ calculated from the theory of Van Vleck (1948). When the crystal was first rotated about an axis perpendicular to $\boldsymbol{H}_0(\beta = \frac{1}{2}\pi)$, the spectrum was indeed halved in width with sidebands appearing at $2\omega_{\mathrm{r}}$ (Andrew *et al.* 1958*a*, *b*), as illustrated in figure 3. Then by rotating the crystal at the magic angle ($\beta = 54^\circ\,44'$), the central line did indeed narrow very sharply with spinning

† It was at the Ampere Congress in Pisa in 1960, where we presented some of our results, that the late Professor C. J. Gorter of Leiden asked a question about the 'magic' properties of this angle which led us to use this terminology thereafter.

sidebands appearing at multiples of ω_r (Andrew *et al.* 1959), also shown in figure 3. These spectra were obtained before the days of Fourier transform n.m.r. spectrometers and appear as derivative spectra as was customary from wideline n.m.r. spectrometers at that time. The variations of the width of the central spectrum followed the reduction factor $F(\beta)$ (equation (7))

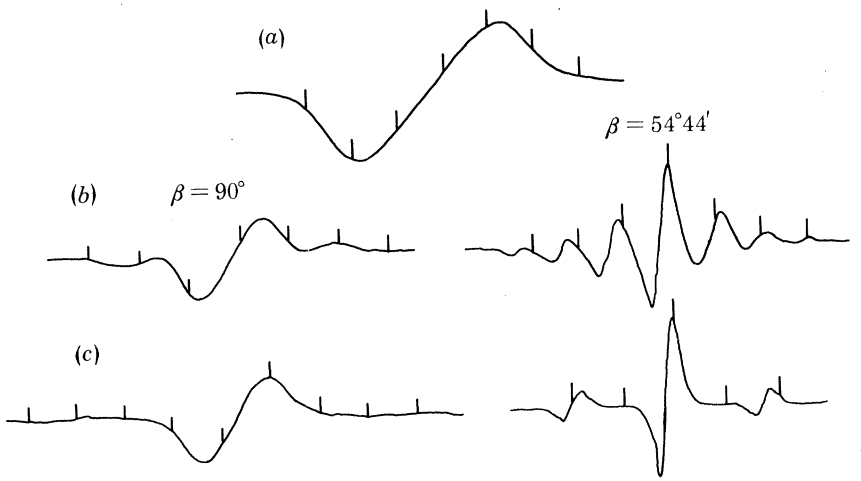

FIGURE 3. The effect of rapid rotation of a solid on its dipolar-broadened spectrum. ^{23}Na n.m.r. derivative spectra of monocrystalline sodium chloride. Markers are at 800 Hz intervals. (*a*) Static crystal; (*b*), (*c*) recordings with the crystal spinning at 800 and 1600 Hz respectively. The left-hand pair of recordings were obtained with the rotation axis perpendicular to the magnetic field. The right-hand pair were obtained with the rotation axis inclined at the magic angle of 54° 44′ to $\boldsymbol{H}_0$ (Andrew *et al.* 1958*a*, *b*, 1959).

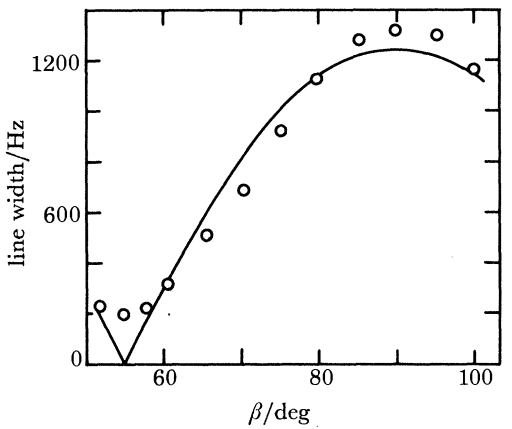

FIGURE 4. Variation of linewidth of ^{23}Na n.m.r. spectrum of a rotating crystal of sodium chloride with the angle β. The full line is the theoretical curve given by (7); the circles are the experimental observations (Andrew *et al.* 1959).

quite well, as shown in figure 4. The linewidth at the magic angle was 200 Hz, largely determined by field inhomogeneity of the wideline spectrometer; magic angle line widths as narrow as a few hertz have since been obtained by using high-resolution magnets. Early verification of these ideas was independently made by Lowe (1959), who used a crystal of calcium fluoride and a sample of polytetrafluoroethylene.

A good example of the removal of dipolar broadening by magic angle spinning is provided by the ^{27}Al n.m.r. spectrum of polycrystalline aluminium metal (Andrew *et al.* 1973, 1974*a*). As

illustrated in figure 5, the spectrum of the static material is about 10 kHz broad. Magic angle spinning at 7.7 kHz reduced this width to about 400 Hz. This enabled the isotropic Knight shift to be measured with very much improved precision, yielding a value of $1640 \pm 1 \times 10^{-6}$ relative to $AlCl_3$ solution at 298 K. A similar improvement in the precision of measuring isotropic Knight shifts was obtained for ^{63}Cu and ^{65}Cu in polycrystalline copper metal (Andrew *et al.* 1971*a*; Andrew 1973).

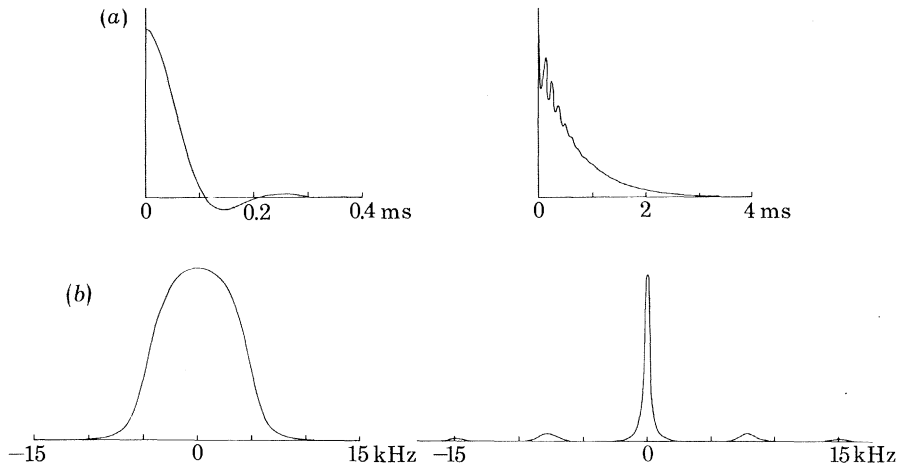

FIGURE 5. ^{27}Al free induction decays (*a*) and Fourier-transformed n.m.r. spectra (*b*) of polycrystalline aluminium. The left-hand diagrams refer to the static specimen; the right-hand diagrams refer to the specimen spinning about the magic axis at 7.7 kHz. Two rotation sidebands are seen on either side of the narrowed central line (Andrew *et al.* 1973, 1974*a*).

3. Magic angle spinning and anisotropic shift interactions

The electron shielding or shift interaction of nuclei in non-metals may be written

$$\mathscr{H}_s = \hbar \sum_i (\boldsymbol{I}_i \cdot \boldsymbol{\sigma}_i \cdot \boldsymbol{H}_0), \tag{8}$$

where $\boldsymbol{\sigma}_i$ is the chemical shift tensor of nucleus i. In metals the shift interaction is conventionally defined with opposite sign

$$\mathscr{H}_s = -\hbar \sum_i (\boldsymbol{I}_i \cdot \boldsymbol{K}_i \cdot \boldsymbol{H}_0), \tag{9}$$

where $\boldsymbol{K}_i$ is the Knight shift tensor of nucleus i. Apart from this difference in sign, the behaviour of $\boldsymbol{\sigma}$ and $\boldsymbol{K}$ is the same in what follows.

We note that $\boldsymbol{\sigma}$ and $\boldsymbol{K}$ are second-rank tensors, but unlike the dipolar interaction tensor, which is a traceless, axially symmetric tensor, $\boldsymbol{\sigma}$ and $\boldsymbol{K}$ are not traceless, are not necessarily axially symmetric, and may not even necessarily be symmetric. However, any antisymmetric components have negligible effects on the spectrum (Haeberlen 1976) and will be neglected.

Since the components of the shift tensor are in practice small compared with unity we need only retain σ_{izz} and rewrite (8) as

$$\mathscr{H}_s = \hbar \sum_i \gamma_i \sigma_{izz} H_0. \tag{10}$$

If the principal values of $\boldsymbol{\sigma}$ are σ_p ($p = 1, 2, 3$) and the direction cosines of its principal axes with respect to $\boldsymbol{H}_0$ are λ_p, then dropping the suffix i for simplicity,

$$\sigma_{zz} = \sum_p \lambda_p^2 \sigma_p. \tag{11}$$

Since the isotropic average of each λ_p^2 is $\frac{1}{3}$, the average value of σ_{zz} in a normal fluid is

$$\bar{\sigma}_{zz} = \tfrac{1}{3}\,\mathrm{tr}\,\boldsymbol{\sigma} = \sigma, \tag{12}$$

where σ is the scalar chemical shift encountered in high-resolution n.m.r. spectra of fluids.

When a rigid array of nuclei in a solid is rotated with angular velocity ω_r about an axis inclined at angle β to $\boldsymbol{H}_0$ and at angles χ_p to the principal axes of σ we have (cf. equation (3))

$$\lambda_p = \cos\beta\cos\chi_p + \sin\beta\sin\chi_p\cos(\omega_r t + \psi_p). \tag{13}$$

From (10), (11) and (13) we see that a time dependence is imposed on $\mathscr{H}_s$, and as with the dipolar interaction we may decompose $\mathscr{H}_s$ into its mean value $\overline{\mathscr{H}}_s$ and terms periodic in ω_r which generate spinning sidebands. Substituting (13) into (11) and taking the time average we find for each nucleus

$$\bar{\sigma}_{zz} = \tfrac{3}{2}\sigma\sin^2\beta + \tfrac{1}{2}(3\cos^2\beta - 1)\sum_p \sigma_p\cos^2\chi_p. \tag{14}$$

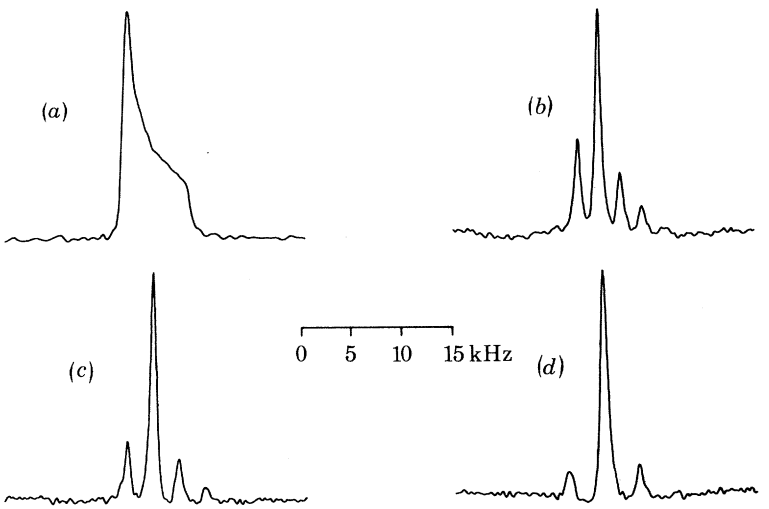

FIGURE 6. The removal of shift anisotropy by magic angle spinning. ^{111}Cd n.m.r. spectra of polycrystalline cadmium metal, (*a*) static and rotating about the magic axis at (*b*) 2.1, (*c*) 2.6 and (*d*) 3.6 kHz (Andrew *et al.* 1974*a*, *b*).

Consequently when β is the magic angle, $\arccos\frac{1}{\sqrt{3}}$, we see that $\bar{\sigma}_{zz}$ reduces to the scalar isotropic value σ, and shift anisotropy is removed from the n.m.r. spectrum for every nucleus in the specimen whatever the degree of anisotropy or asymmetry of its shift tensor and whatever the orientation of its principal axes. This result, demonstrating that magic angle spinning removes shift anisotropy, was first derived by Andrew & Wynn (1966) (see also Andrew 1971).

The time-averaged shift given in (14) may be re-expressed in terms of the anisotropy parameter $\delta = \sigma_3 - \sigma$ and the asymmetry parameter $\eta = (\sigma_2 - \sigma_1)/\delta$ of each nucleus, introduced by Lippmaa *et al.* (1976). Substituting these parameters in (14) and rearranging we get

$$\bar{\sigma}_{zz} = \sigma + \tfrac{1}{2}(3\cos^2\beta - 1)\,\delta\{\tfrac{1}{2}(3\cos^2\theta' - 1) + \tfrac{1}{2}\eta\sin^2\theta'\cos 2\phi'\}, \tag{15}$$

where θ' and ϕ' are spherical polar angles relating the specimen rotation axis to the principal axes of the shift tensor ($\chi_3 = \theta'$; $\cos\chi_2 = \sin\theta'\cos\phi'$; $\cos\chi_1 = \sin\theta'\sin\phi'$). Expressed in this form we see in a direct manner how the ubiquitous Legendre factor $\frac{1}{2}(3\cos^2\beta - 1)$ controls the shift anisotropy in the time-averaged Hamiltonian $\overline{\mathscr{H}}_s$, for every nucleus in the specimen.

An experimental example of the removal of shift anisotropy by magic angle spinning is provided by cadmium, a metal with a hexagonal crystal structure. The ^{111}Cd n.m.r. spectra of a polycrystalline specimen of cadmium metal are shown in figure 6 (Andrew *et al.* 1974*a*, *b*). The spectrum for the static material shows the asymmetric profile characteristic of an axially symmetric shift tensor. Dipolar broadening is small in this material on account of the low isotopic abundance (12 %) and the low nuclear magnetic moment ($-0.6\mu_n$); the Knight shift anisotropy is the dominant source of n.m.r. broadening in the powder. Also shown in figure 6 are spectra for three spinning rates. It is seen that magic angle spinning removes the anistropy and it enables the isotropic Knight shift to be obtained with precision ($4321 \pm 7 \times 10^{-6}$ for ^{111}Cd, $4324 \pm 7 \times 10^{-6}$ for ^{113}Cd, relative to cadmium nitrate solution). It is believed that this was the first experimental demonstration of the removal of shift anisotropy by magic angle spinning.

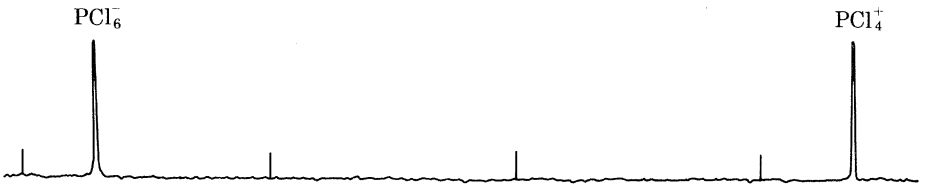

FIGURE 7. ^{31}P n.m.r. spectrum of polycrystalline phosphorus pentachloride with magic angle spinning. The two lines arise from the differently shielded PCl_4^+ and PCl_6^- ions of which the solid is composed. Markers at 1 kHz intervals (Andrew *et al.* 1960*a*, *b*, 1966).

A new feature is to be noticed in figure 6. Unlike the dipolar broadened spectra, where the rotation rate must be comparable with the line width to get substantial narrowing, here we see that the line breaks up almost immediately into an array of satellites each of narrow breadth. This was subsequently noticed for non-metals by Schaefer & Stejskal (1976) and by Lippmaa *et al.* (1976). The essential difference is that here the line is inhomogeneously broadened. Each element of the spectrum of the static specimen arises from crystallites of a particular orientation, each with small intrinsic width. The situation is closely analogous to the n.m.r. line from a liquid broadened by an inhomogeneous magnetic field; each volume element in the sample contributes its own portion to the spectrum. The intrinsic width of the spectrum may then be recovered from the decay of the spin-echo envelope (Hahn 1950). Analogous rotational echoes have been observed by Maricq & Waugh (1977), and the decay envelope of such echoes gives the intrinsic width of each shifted spin packet. In a subsequent paper Maricq & Waugh (1979) have discussed the behaviour of such rotational spin echoes in terms of average Hamiltonian theory (Haeberlen & Waugh 1968), from which it is seen that the criterion for precise averaging with slow rotations is that the terms in the interaction Hamiltonian commute. If chemical shift interactions dominate, the terms commute and the spectrum is inhomogeneous; if dipolar or pseudo-dipolar terms are important the terms do not commute, the line is homogeneous, and higher rotation rates are required to achieve effective narrowing.

Even though slower rates of rotation narrow inhomogeneously broadened spectra, in the interests of good signal intensity it is of course still necessary to spin the specimen at a rate fast compared with the static line width to make the sidebands unobservably weak and concentrate all the intensity onto the central line.

Chemically shifted fine structures have been resolved in the ^{31}P n.m.r. spectra of a number of polycrystalline phosphorus compounds by using magic angle spinning (Andrew & Wynn 1966;

PHILOSOPHICAL TRANSACTIONS OF THE ROYAL SOCIETY A MATHEMATICAL, PHYSICAL & ENGINEERING SCIENCES

Kessemeier & Norberg 1967; Andrew *et al.* 1976). In solid phosphorus pentachloride two well resolved lines reduced to 10 Hz breadth by fast magic angle spinning were obtained from the differently shielded PCl_4^+ and PCl_6^- ions of which this solid is composed, and this enabled interesting cross-relaxation effects to be examined (Andrew *et al.* 1960*a*, *b*, 1963, 1966). The ^{31}P n.m.r. spectrum of the rapidly rotated solid is shown in figure 7. This is an excellent example of a material that has a different molecular structure in the solid and the liquid states. In CS_2 solution it has the molecular form PCl_5, giving a single resonance line. Taken with the measured shift for liquid PCl_3, we have the following monotonic sequence of chemical shifts for the four phosphorus chlorides relative to 85 % orthophosphoric acid solution:

PCl_3	PCl_4^+	PCl_5	PCl_6^-
-215	-91	$+80$	$+282\times10^{-6}$.

4. Magic angle spinning and anisotropic interactions

In the two previous sections we have shown from first principles that fast specimen spinning about an axis inclined at angle β to $\boldsymbol{H}_0$ introduces a factor $\frac{1}{2}(3\cos^2\beta-1)$ into the time-averaged Hamiltonian representing the dipolar interaction and also into that representing the anisotropic shift interaction. It will therefore not surprise the reader that similar calculations from first principles show that the same factor appears in the time-averaged Hamiltonian representing the anisotropic electron-coupled spin–spin interaction (Andrew & Farnell 1968) and in that representing the first-order electric quadrupolar interaction (Cunningham & Day 1966), and that magic angle spinning should therefore remove all these symmetric second-rank tensor interactions. This suggests that all these interactions could be treated in a common formalism.

The various interactions may be written as

$$\text{direct dipolar interaction, } \mathscr{H}_\mathrm{d} = \sum_{i<j} \boldsymbol{I}_i\cdot\boldsymbol{D}_{ij}\cdot\boldsymbol{I}_j; \tag{16}$$

$$\text{indirect electron-coupled interaction, } \mathscr{H}_\mathrm{J} = h\sum_{i<j} \boldsymbol{I}_i\cdot\boldsymbol{J}_{ij}\cdot\boldsymbol{I}_j; \tag{17}$$

$$\text{electron shielding, non-metals, } \mathscr{H}_\mathrm{s} = \hbar\sum_{i} \boldsymbol{I}_i\cdot\boldsymbol{\sigma}_i\cdot\boldsymbol{H}_0; \tag{18}$$

$$\text{electron shielding, metals, } \mathscr{H}_\mathrm{s} = -\hbar\sum_{i} \boldsymbol{I}_i\cdot\boldsymbol{K}_i\cdot\boldsymbol{H}_0; \tag{19}$$

$$\text{electric quadrupolar interaction, } \mathscr{H}_\mathrm{q} = \sum_{i} \frac{eQ_i}{6I_i(2I_i-1)}\,\boldsymbol{I}_i\cdot\boldsymbol{V}_i\cdot\boldsymbol{I}_i. \tag{20}$$

Equation (16) is an alternative expression of (1), where $\boldsymbol{D}_{ij}$ is the truncated dipolar interaction tensor between nuclei i and j. In (17), $\boldsymbol{J}_{ij}$ is the electron-coupled spin–spin interaction tensor between nuclei i and j. In (20), eQ_i is the nuclear electric quadrupole moment of nucleus i and $\boldsymbol{V}_i$ is the electric field gradient tensor at its site.

$\boldsymbol{D}_{ij}$, $\boldsymbol{J}_{ij}$, $\boldsymbol{\sigma}_i$, $\boldsymbol{K}_i$, $\boldsymbol{V}_i$ are all second-rank tensors. $\boldsymbol{D}_{ij}$ is axially symmetric and traceless; $\boldsymbol{V}_i$ is symmetric and traceless; the others are not restricted. We shall, however, continue to neglect any antisymmetric component of tensors $\boldsymbol{\sigma}_i$, $\boldsymbol{K}_i$ and $\boldsymbol{J}_{ij}$, and we can render them all traceless by the simple expedient of subtracting their constant isotropic trace. Thus

$$\boldsymbol{J} = J\boldsymbol{1}+\boldsymbol{J}^* \quad \text{where} \quad J = \tfrac{1}{3}\mathrm{tr}\,\boldsymbol{J}; \tag{21}$$

$$\boldsymbol{\sigma} = \sigma\boldsymbol{1}+\boldsymbol{\sigma}^* \quad \text{where} \quad \sigma = \tfrac{1}{3}\mathrm{tr}\,\boldsymbol{\sigma}; \tag{22}$$

$$\boldsymbol{K} = K\boldsymbol{1}+\boldsymbol{K}^* \quad \text{where} \quad K = \tfrac{1}{3}\mathrm{tr}\,\boldsymbol{K}. \tag{23}$$

In these expressions **1** is the unit tensor, and J, σ and K are the isotropic coupling constants and shifts encountered in isotropic liquids. The tensors $\boldsymbol{J}^*$, $\boldsymbol{\sigma}^*$, $\boldsymbol{K}^*$ are all traceless symmetric tensors representing the anisotropic properties of these interactions.

These five second-rank tensor interactions represented by (16)–(23) all have a common structure and as Haeberlen (1976) has shown, they may be cast in a common form in terms of their irreducible tensor operators:

$$\mathscr{H}_\lambda = C^\lambda \sum_l \sum_{m=-l}^{l} (-1)^m R^\lambda_{l,-m} T^\lambda_{lm} \tag{24}$$

in which C^λ are constants specific to each interaction, the terms $R^\lambda_{l,-m}$ are angular functions in coordinate space and the terms T^λ_{lm} are spin products. Since we are dealing with traceless symmetric second-rank tensors, only $R^\lambda_{l,-m}$ terms with $l = 2$ and $m = 0, \pm 2$ are non-zero.

We now need to express the tensor components $R^\lambda_{2,-m}$ for each nucleus or pair of nuclei in the laboratory frame in terms of its components in a convenient crystal frame of reference rotating in the laboratory frame. Next these components in the crystal frame need to be expressed in terms of the invariant principal values of the tensor in its principal axis frame. These two transformations are conveniently accomplished by using the Wigner rotation matrices $\mathscr{D}^l_{m'm}(\alpha, \beta, \gamma)$, where α, β, γ are the Euler angles relating the frames of reference. The number of terms in this double transformation is severely limited since in calculating the spectra we are restricted to terms T^λ_{lm} in the Hamiltonian that are secular, $m = 0$. In the transformation from the crystal frame to the laboratory frame we are left with Wigner rotation matrices of the form $\mathscr{D}^2_{m'0}(0, \beta, \omega_r t)$; as before, β is the angle between the spinning axis and $\boldsymbol{H}_0$. If one now consults a table of Wigner rotation matrices, and notes that those with factors $e^{\pm i\omega_r t}$, $e^{\pm 2i\omega_r t}$ average to zero under fast rotation, we find only one non-zero rotation matrix is left, namely

$$\mathscr{D}^2_{00}(0, \beta, \omega_r t) = \tfrac{1}{2}(3\cos^2\beta - 1). \tag{25}$$

Thus all terms in the time-averaged Hamiltonians $\overline{\mathscr{H}_\lambda}$, for all five traceless tensor interactions, contain this factor (25). When β is the magic angle, $\arccos \frac{1}{\sqrt{3}} = 54° 44'$, all these interactions therefore vanish from the spectrum under fast rotation.

5. Magic angle spinning and indirect spin–spin interactions

The removal of anisotropic broadening interactions by magic angle spinning frequently reveals fine structure previously obscured. An example is given in figure 8, which shows the ^{19}F n.m.r. spectrum of polycrystalline potassium hexafluoroarsenate, $KAsF_6$ (Andrew *et al.* 1967). The spectrum from the static material is about 15 kHz broad. Magic angle spinning at 5.5 kHz largely removed the anisotropic sources of broadening ($\boldsymbol{D}$, $\boldsymbol{J}^*$, $\boldsymbol{\sigma}^*$) and resolved a spin quartet, with an isotropic coupling constant, J, of 905 Hz. The quartet arises from the coupling of the ^{19}F nuclei with the 100 % abundant ^{75}As nucleus in the octahedral AsF_6^- ions in the solid. This was in fact the first spin multiplet to be resolved in the n.m.r. spectrum of a solid by any method.

Another example is given in figure 9, which shows the ^{19}F spectrum of polycrystalline potassium hexafluorophosphate, KPF_6, both static and with magic angle spinning at 8 kHz (Andrew *et al.* 1970). Again the spectrum of the static material is about 15 kHz wide; the spectrum with spinning resolves a doublet arising from indirect ^{19}F–^{31}P spin–spin coupling in

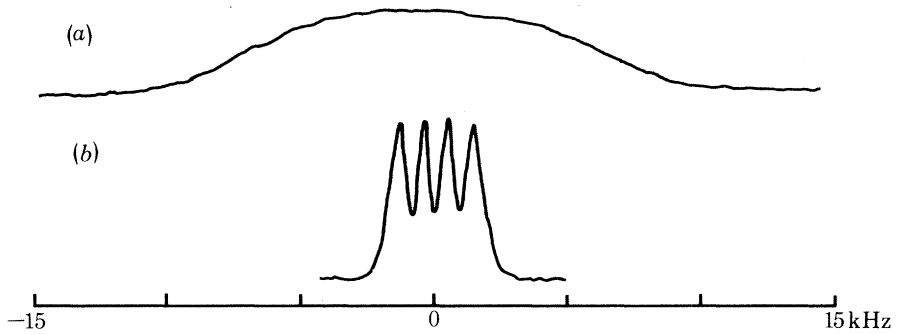

FIGURE 8. A spin multiplet resolved in the solid state by magic angle spinning. ^{19}F n.m.r. spectra of polycrystalline $KAsF_6$. (*a*) Static specimen; (*b*) specimen spinning at 5.5 kHz, displaying quartet structure due to *J* coupling between ^{19}F and ^{75}As nuclei (Andrew *et al.* 1967).

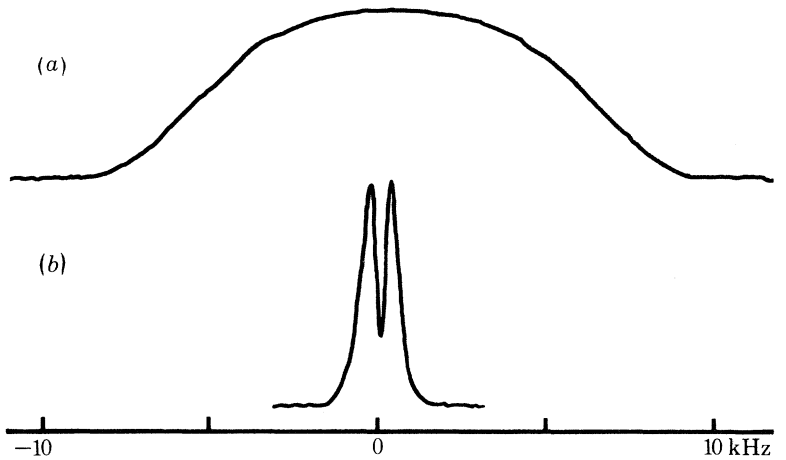

FIGURE 9. A spin doublet resolved in the solid state by magic angle spinning. ^{19}F n.m.r. spectra of polycrystalline KPF_6. (*a*) Static specimen; (*b*) specimen spinning at 8 kHz revealing a doublet due to *J* coupling between ^{19}F and ^{31}P nuclei (Andrew *et al.* 1970).

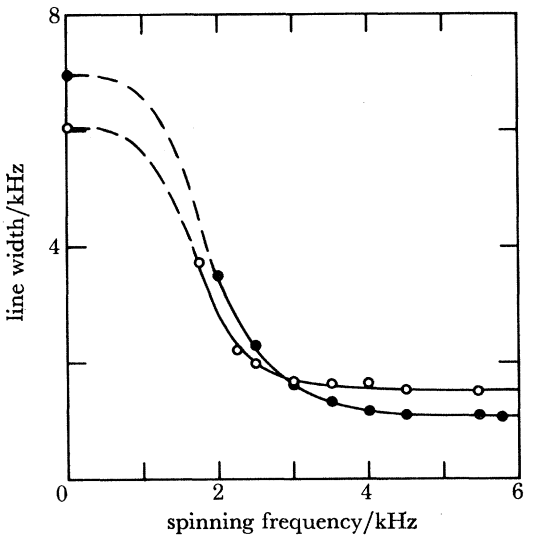

FIGURE 10. N.m.r. line widths for copper metal as a function of spinning frequency ●, ^{63}Cu; ○, ^{65}Cu (Andrew *et al.* 1971*b*). The rotationally invariant line widths above 4 kHz arise from the Ruderman–Kittel interaction.

the PF_6^- ions ($J = 743$ Hz). In polycrystalline potassium hexafluoroantimonate a ^{19}F–^{121}Sb sextet and a ^{19}F–^{123}Sb octet have also been resolved (Andrew *et al.* 1970).

Electron-coupled spin–spin interactions also exhibit themselves in the narrowed n.m.r. spectra of metallic copper. As shown in figure 10, magic angle spinning substantially reduces the ^{63}Cu and ^{65}Cu line widths, but for rotation rates above 3 kHz a constant limiting linewidth is reached that is evidently due to a rotationally invariant interaction (Andrew *et al.* 1971*b*; Andrew 1973). By comparing the second moments of the residual lines and finding them to be in the inverse ratio of the abundances of the two copper isotopes, it was shown that these residual breadths were due to the Ruderman–Kittel electron-coupled interactions. A value of $J = 230 \pm 10$ Hz was extracted for the nearest-neighbour coupling constants, in reasonable agreement with theory, and consistent with the value for silver (Andrew & Hinshaw 1973).

TABLE 1. MAGIC ANGLE SPINNING AND QUADRUPOLE INTERACTIONS

solid compound	line width/Hz: static	line width/Hz: rotating (3 kHz)	line width ratio
Cs_2SO_4	1060	60	18
Cs_2CO_3	1270	180	7

6. MAGIC ANGLE SPINNING AND NUCLEAR QUADRUPOLE INTERACTIONS

It was shown in §4 that fast magic angle spinning should also average the quadrupolar Hamiltonian $\mathscr{H}_q$ to a small value. This is not an easy interaction to put to an experimental test since quadrupole interactions in non-cubic environments tend to be large. Even if less than the Zeeman interaction, first-order perturbation theory is often not a sufficient approximation and second-order contributions may need consideration (Maricq & Waugh 1979). On the other hand, the smaller quadrupole couplings found in nominally cubic environments may be hard to distinguish from comparable dipolar interactions (Cunningham & Day 1966).

However, an unequivocal test was carried out by Tzalmona & Andrew (1974) using two polycrystalline non-cubic caesium salts, Cs_2SO_4 and Cs_2CO_3. ^{133}Cs, which has 100 % abundance and spin $\frac{7}{2}$, has an unusually small electric quadrupole moment, -3×10^{-27} cm^2. Consequently the quadrupole broadening in these salts was of order 10^3 Hz, and first-order theory suffices to describe it. Moreover, since the nearest-neighbour separation of the caesium atoms is about 4 Å (0.4 nm), and there are no other abundant magnetic nuclei in these solids, the dipolar contribution to the line width is an order of magnitude smaller than the quadrupolar contribution. The results are summarized in table 1. It is seen that magic angle spinning does substantially narrow the quadrupolar broadened lines in both solids.

7. MACROSCOPIC AND MICROSCOPIC MOTIONS

A question frequently asked is whether magic angle spinning can narrow an n.m.r. spectrum which is already partly narrowed by molecular or ionic motion within the solid. This situation has been examined by Andrew & Jasinski (1971), and two different situations may be distinguished. The first may be called 'fast restricted motion' and the second 'slow or moderate isotropic motion'.

In the first, fast restricted motion, for example by the random reorientation of molecules or groups in the solid about one axis, leads to a reduced plateau value of the second moment. In

PHILOSOPHICAL TRANSACTIONS OF THE ROYAL SOCIETY A MATHEMATICAL, PHYSICAL & ENGINEERING SCIENCES

such a case, when the specimen is spun about the magic axis the average interaction Hamiltonians must be found by taking the time average over both macroscopic and microscopic motions, and it is found that the anisotropic interactions all average to zero. This conclusion is in agreement with experiment, for example with polytetrafluoroethylene (Lowe 1959; Andrew 1970). The ^{19}F n.m.r. spectrum at room temperature is already narrowed to about 30 % of its low-temperature rigid-structure width, and magic angle spinning removes the remaining breadth associated with other degrees of molecular freedom. In such cases the microscopic molecular motion makes the task of macroscopic narrowing easier, since the rate of rotation need only be comparable with the already reduced line width.

In the second situation, substantial spectral narrowing has been achieved by isotropic molecular rotation and diffusion. All degrees of freedom of the molecules are mobilized, but the rate of motion, though fast enough to narrow the spectrum substantially, is not fast enough to give the really sharp lines characteristic of mobile liquids. For example, an internal motion with correlation frequency 10^6 Hz might narrow a line of rigid-lattice width 10^4 Hz to an observed width of 10^2 Hz. In this case macroscopic spinning at 10^2 Hz will have no effect on the residual line width, nor even at 10^4 Hz. The rate of magic angle spinning would have to be greater than the internal motion, 10^6 Hz in our example, to produce further narrowing of the line, and that is impracticable. With this class of materials, internal microscopic molecular motion is a hindrance and not a help in securing very narrow lines. It should be noted that this limitation to the achievement of high-resolution n.m.r. in solids applies equally to other methods of line narrowing in solids (Haeberlen & Waugh 1968).

There are, of course, intermediate situations between these two extreme types of behaviour, and this enables information to be obtained about internal motions present; in particular it has been used in studies of molecular motions in polymers (Schneider *et al.* 1972; Pivcova *et al.* 1974).

8. Factors affecting resolution

Many factors determine the ultimate width of the n.m.r. lines narrowed by magic angle spinning. A discussion of most of these factors has been given previously (Andrew 1971), and we may therefore content ourselves here with a list of the more important ones (table 2).

Table 2. Factors affecting resolution in magic angle spinning

(*a*) *instrumental factors*
inhomogeneity of the laboratory magnetic field, H_0
imperfect adjustment to the magic angle
insufficiently fast spinning
bulk susceptibility effects
(*b*) *residual interactions*
residual dipolar and pseudo-dipolar interactions
chemical shift distributions
intermolecular J couplings
Ruderman–Kittel interactions
antisymmetric tensor interactions
quadrupole effects
higher-order multipole interactions
(*c*) *motional and relaxation effects*
spin-lattice relaxation
cross-relaxation
slow internal motions

9. Spinners

The type of spinner used in our work is illustrated in figure 11 (Andrew *et al.* 1969). It is based on a type introduced by Henriot & Huguenard (1925, 1927) and developed by Beams (1930, 1937). Our particular contribution was to make the rotors out of non-metallic materials for use in a magnetic field, to incorporate a specimen chamber into the rotor and to adapt the system for use in an n.m.r. spectrometer probe.

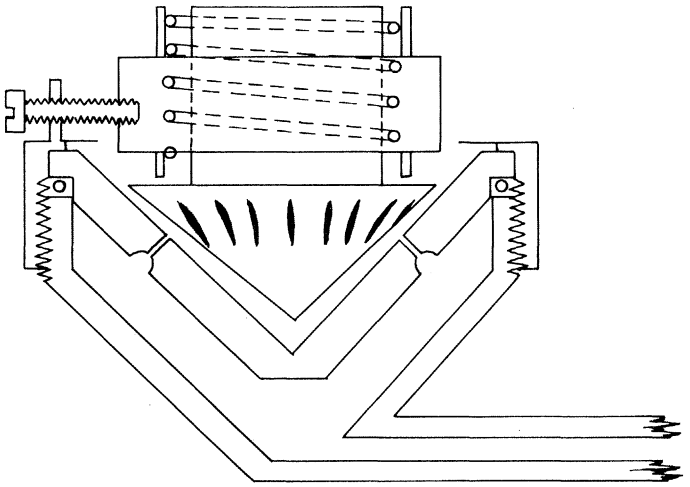

Figure 11. Turbine assembly for magic angle spinning (Andrew *et al.* 1969).

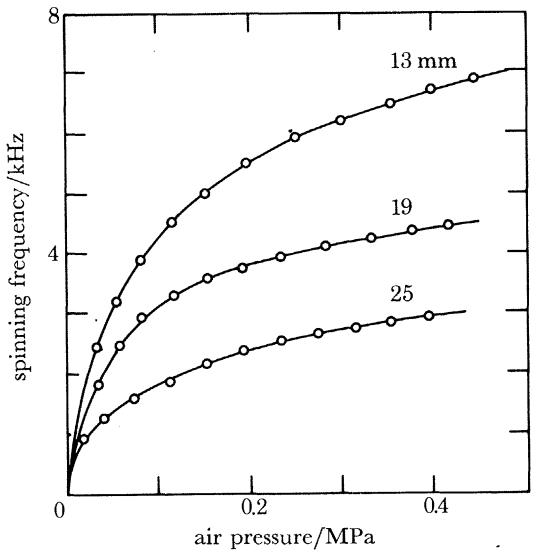

Figure 12. Variation of spinning frequency with air pressure for turbines of the type shown in figure 11, with nylon rotors of diameter 13, 19 and 25 mm.

The turbine is driven by compressed gas, which emerges through inclined jets machined in the stator and impinges on the conical underside of the rotor, which is provided with a set of flutes. The rotor is thus supported on a gas bearing and rotates with little frictional resistance. The specimen chamber is on top of the rotor and is an integral part of the rotor construction;

it spins freely within the radio-frequency coil of the n.m.r. spectrometer, with a good filling factor.

Such rotors spin with great stability. They will rotate about an axis inclined at any angle to the vertical, even upside down; however, they start most readily with the axis vertical. Magic angle spinners of this general type are now found in several commercial n.m.r. spectrometers.

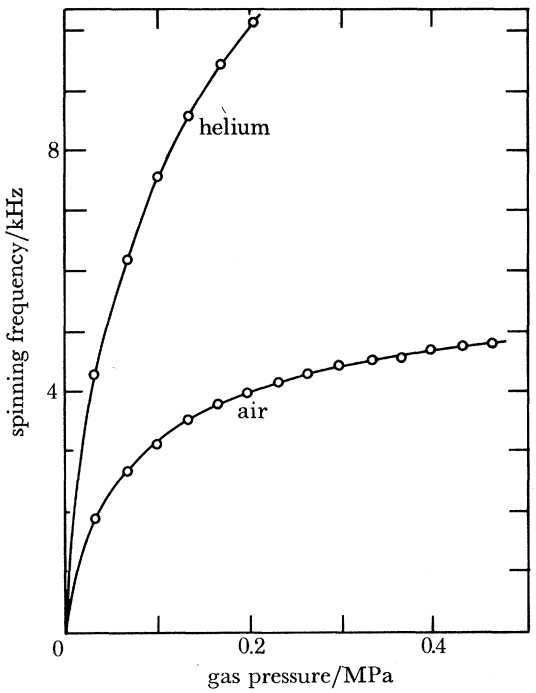

FIGURE 13. Comparison of spinning frequencies for a turbine of the type shown in figure 11 with a nylon rotor 19 mm in diameter when driven by air and by helium.

In figure 12 the variation of rotation rate with air pressure is shown for a family of such spinners with rotor diameters of 13, 19 and 25 mm. At higher pressures the rate of rotation tends towards a limiting value when the peripheral velocity of the rotor approaches the velocity of sound in air. In pursuit of higher rotation rates we have used helium as the propelling gas since the velocity of sound therein is 2.7 times higher than that of air. The remarkable increase of rotation rate attained with the use of helium gas is illustrated in figure 13 for a 19 mm diameter rotor. The highest frequency of rotation achieved with a spinner of this type was 13 kHz.

At a rotation frequency of 10 kHz (600000 revolutions per minute), the peripheral velocity of a 19 mm rotor is 6×10^4 cm s^{-1} (2000 km h^{-1}), and the peripheral acceleration is 4×10^6 g. The rotors must therefore be made of strong materials. Nylon was the strongest homogeneous material used. For the highest rotation frequencies, glass-fibre and carbon-fibre reinforced materials were used.

This paper was written while the author was a visiting scientist at the C.E.N.G. Laboratory, Grenoble, France, in the summer of 1980, and he wishes to express his warm thanks to Dr Pierre Servoz-Gavin and his colleagues in the Section de Résonance Magnétique for their kind hospitality.

References (Andrew)

Andrew, E. R. 1959 *Archs Sci., Genève* **12**, fasc. spéc., 103–108.
Andrew, E. R. 1970 In *Magnetic resonance* (ed. C. K. Coogan *et al.*), pp. 163–176. Plenum Press.
Andrew, E. R. 1971 *Prog. nucl. magn. Reson. Spectr.* **8**, 1–39.
Andrew, E. R. 1973 In *Proc. 17th Congress Ampere*, Turku, pp. 18–32. Amsterdam: North-Holland.
Andrew, E. R. 1975 In *International review of science, Physical Chemistry* ser. 2, vol. 4 (*Magnetic resonance*) (ed. C. A. McDowell), pp. 173–208. London: Butterworths.
Andrew, E. R., Bradbury, A. & Eades, R. G. 1958*a* *Nature, Lond.* **182**, 1659.
Andrew, E. R., Bradbury, A. & Eades, R. G. 1958*b* *Archs Sci., Genève* **11**, fasc. spéc., 223–226.
Andrew, E. R., Bradbury, A. & Eades, R. G. 1959 *Nature, Lond.* **183**, 1802–1803.
Andrew, E. R., Bradbury, A., Eades, R. G. & Jenks, G. J. 1960*a* *Nature, Lond.* **188**, 1096–1097.
Andrew, E. R., Bradbury, A., Eades, R. G. & Jenks, G. J. 1960*b* *Bull. Ampere*, **9**, fasc. spéc., 371–373.
Andrew, E. R., Bradbury, A., Eades, R. G. & Wynn, V. T. 1963 *Phys. Lett.* **4**, 99–100.
Andrew, E. R., Carolan, J, L. & Randall, P. J. 1971*a* *Phys. Lett.* A **35**, 435–436.
Andrew, E. R., Carolan, J. L. & Randall, P. J. 1971*b* *Phys. Lett.* A **37**, 125–126.
Andrew, E. R., Clough, S., Farnell, L. F., Gledhill, T. D. & Roberts, I. 1966 *Phys. Lett.* **21**, 505–506.
Andrew, E. R. & Farnell, L. F. 1968 *Molec. Phys.* **15**, 157–165.
Andrew, E. R., Farnell, L. F. & Gledhill, T. D. 1967 *Phys. Rev. Lett.* **19**, 6–7.
Andrew, E. R., Farnell, L. F., Firth, M., Gledhill, T. D. & Roberts, I. 1969 *J. magn. Reson.* **1**, 27–34.
Andrew, E. R., Firth, M., Jasinski, A. & Randall, P. J. 1970 *Phys. Lett.* A **31**, 446–447.
Andrew, E. R. & Hinshaw, W. S. 1973 *Phys. Lett.* A **43**, 113–114.
Andrew, E. R., Hinshaw, W. S., Hutchins, M. G. & Jasinski A. 1978 *Proc. R. Soc. Lond.* A **364**, 553–567.
Andrew, E. R., Hinshaw, W. S. Jasinski, A. 1974*c* *Chem. Phys. Lett.* **24**, 399–401.
Andrew, E. R., Hinshaw, W. S. & Tiffen, R. S. 1973 *Phys. Lett.* A **46**, 57–58.
Andrew, E. R., Hinshaw, W. S. & Tiffen, R. S. 1974*a* *J. magn. Reson.* **15**, 191–195.
Andrew, E. R., Hinshaw, W. S. & Tiffen, R. S. 1974*b* In *Proc. 18th Ampere Congress*, Nottingham, pp. 325–326. Amsterdam: North-Holland.
Andrew, E. R. & Jasinski, A. 1971 *J. Phys.* C **4**, 391–400.
Andrew, E. R. & Jenks, G. J. 1962 *Proc. phys. Soc.* **80**, 663–673.
Andrew, E. R. & Newing, R. A. 1958 *Proc. Phys. Soc.* **72**, 959–972.
Andrew, E. R., Vennart, W., Bonnard, G., Croiset, R. M., Demarcq, M. & Mathieu, E. 1976 *Chem. Phys. Lett.* **43**, 317–320.
Andrew, E. R. & Wynn, V. T. 1966 *Proc. R. Soc. Lond.* A **291**, 257–266.
Beams, J. W. 1930 *Rev. scient. Instrum.* **1**, 667–671.
Beams, J. W. 1937 *J. appl. Phys.* **8**, 795–806.
Cunningham, A. C. & Day, S. M. 1966 *Phys. Rev.* **152**, 287–292.
Haeberlen, U. 1976 *High resolution NMR in solids* (*Adv. magn. Reson., Suppl.* 1). New York: Academic Press.
Haeberlen, U. & Waugh, J. S. 1968 *Phys. Rev.* **175**, 453–467.
Hahn, E. L. 1950 *Phys. Rev.* **80**, 580–581.
Henriot, E. & Huguenard, E. 1925 *C.r. hebd. Séanc. acad. Sci., Paris* **180**, 1389–1392.
Henriot, E. & Huguenard, E. 1927 *J. Phys. Radium* **8**, 433–443.
Kessemeier, H. & Norberg, R. E. 1967 *Phys. Rev.* **155**, 321–337.
Lippmaa, E., Alla, M. & Tuherm, T. 1976 In *Proc. 19th Congress Ampere*, Heidelberg, pp. 113–118.
Lowe, I. J. 1959 *Phys. Rev. Lett.* **2**, 285–287.
Mansfield, P. & Ware, D. 1966 *Phys. Rev. Lett.* **22**, 133–135.
Maricq, M. & Waugh, J. S. 1977 *Chem. Phys. Lett.* **47**, 327–329.
Maricq, M. & Waugh, J. S. 1979 *J. chem. Phys.* **70**, 3300–3316.
Mehring, M. 1976 *High resolution NMR spectroscopy in solids*. Berlin: Springer-Verlag.
Ostroff, E. D. & Waugh, J. S. 1966 *Phys. Rev. Lett.* **16**, 1097–1098.
Pines, A., Gibby, M. G. & Waugh, J. S. 1972 *Chem. Phys. Lett.* **15**, 373–376.
Pivcova, H., Doskocilova, D., Veksli, Z. & Schneider, B. 1974 *J. magn. Reson.* **14**, 182–193.
Schaefer, J. & Stejskal, E. O. 1976 *J. Am. chem. Soc.* **98**, 1031–1032.
Schneider, B., Pivcova, H. & Doskocilova, D. 1972 *Macromolecules* **5**, 120–124.
Tzalmona, A. & Andrew, E. R. 1974 *Proc. 18th Ampere Congress*, Nottingham, pp. 241–242. Amsterdam: North-Holland.
Van Vleck, J. H. 1948 *Phys. Rev.* **74**, 1168–1183.

PHILOSOPHICAL TRANSACTIONS OF THE ROYAL SOCIETY A MATHEMATICAL, PHYSICAL & ENGINEERING SCIENCES